Lab on a Chip

Cite this: *Lab Chip*, 2012, **12**, 948

www.rsc.org/loc

**PAPER**

# A 3D mammalian cell separator biochip†

**Debaditya Choudhury,*[a] William T. Ramsay,[a] Robert Kiss,[b] Nicholas A. Willoughby,[b] Lynn Paterson[a] and Ajoy K. Kar[a]**

***Received 27th September 2011, Accepted 3rd January 2012***
**DOI: 10.1039/c2lc20939j**



The dissimilar cytoskeletal architecture in diverse cell types induces a difference in their deformability that presents a viable approach to separate cells in a non-invasive manner. We report on the design and fabrication of a robust and scalable device capable of separating a heterogeneous population of cells with variable degree of deformability into enriched populations with deformability above a certain threshold. The three dimensional device was fabricated in fused silica by femtosecond laser direct writing combined with selective chemical etching. The separator device was evaluated using promyelocytic HL60 cells. Using flow rates as large as 167 μL $min^{-1}$, throughputs of up to 2800 cells $min^{-1}$ were achieved at the device output. A fluorescence-activated cell sorting (FACS) viability analysis on the cells revealed 81% of the population maintain cellular integrity after passage through the device.

## 1. Introduction

The human anatomy consists of a large number of hierarchical networks that are essentially microfluidic in nature. Unlike conventional macroscopic cell culture and manipulation environments, Lab-on-Chip (LOC) devices offer the unique opportunity to mimic *in vivo* biological systems onto closely resembling *in vitro* microfluidic environments. Miniaturized LOC systems have been reported to offer several advantages including precise control and monitoring of the microenvironment, reduced analysis times, smaller reagent volumes, reduced chemical waste and lowered diagnosis costs. In this respect, recent years have seen the emergence of several microfabricated fluidic systems based on photo and soft lithographic techniques.[1–7] In particular, microfluidic systems capable of sorting both bulk and single cells have been reported by different methods including mechanically controlled hydrodynamic flow switching,[8] micro-component enabled hydrodynamic flow switching,[9] electrophoretic/electro-osmotic methods,[10] magnetic,[11] optical[12] and size based methods.[13,14]

In this paper, we report on the fabrication and demonstration of a 3D, pressure-driven, cell manipulation device that is embedded in fused silica using direct femtosecond laser writing followed by selective wet etching. The device is capable of sorting a heterogeneous population of cells with varied levels of deformability into enriched populations of cells with uniform deformability. Laser writing and selective etching parameters are investigated in order to achieve embedded microchannels with preserved post-etch aspect ratios. As proof of principle, human promyelocytic leukemia cells (HL60) are used to demonstrate that cells can pass through narrow, sub-surface channels fabricated by the aforementioned technique. In addition, the feasibility of the device in delivering a viable population of cells is investigated by collecting the cells at the device output and analysing their integrity using a commercial flow cytometer.

Fused silica was chosen as the substrate material for this work due to several advantages, such as high optical quality, robustness, biological compatibility, thermal stability, a wide transmission window and fully controllable photo-induced selective etching rates by varying irradiation parameters such as energy, translation speed and even polarisation state of writing pulses. It is also known that regions in fused silica modified using femtosecond laser pulses exhibit chemical etching rates sensitive to the polarisation of the pulses.[15] The pulse polarisation can be tailored to write sub-surface structures which can then be etched to obtain microchannels with significant difference in aspect ratio. While single channel optofluidic devices have been successfully demonstrated in the recent past,[16,17] a monolithic multichannel device fabricated using this property has not been reported so far.

## 2. Design and fabrication

### 2.1 Design considerations and working principle

The proposed sorting mechanism relies on the dissimilarities in cytoskeletal architecture that exist in different cell types. The cytoskeleton of most cells is primarily composed of proteins

[a]*SUPA, Department of Physics, School of Engineering & Physical Sciences, Heriot-Watt University, Edinburgh, EH14 4AS, Scotland. E-mail: dc119@hw.ac.uk*
[b]*Department of Chemical Engineering, School of Engineering & Physical Sciences, Heriot-Watt University, Edinburgh, EH14 4AS, Scotland*
† Electronic supplementary information (ESI) available. See DOI: 10.1039/c2lc20939j

which can be thought of as scaffolding that provides shape and structure to the cells. Difference in the cytoskeletal network between various cell types manifests as a discernible variation in cell elasticity.[18] Thus, cells with sparse cytoskeletal architecture are softer than cells with a relatively denser network of proteins making up the cytoskeleton.

A network of appropriately designed microchannels enabling accurate pressure driven flow control provides a method to exploit any difference in cell deformability without the use of external forces such as magnetic or electric fields. As shown in Fig. 1, we present a 'proof of principle' design for the device consisting of a T-junction formed by two microchannels with one inlet port and two outlet ports.

At the junction, these microchannels are linked together by narrow constrictions forming a filter region. If a heterogeneous population of cells is inserted into the device through the inlet and a pressure gradient is maintained across the constrictions, the softer cells will be able to deform and navigate their way through these constrictions into outlet 1 of the device, provided the cross-section of the constrictions is narrower than the average size of a cell. The more rigid cells will be unable to deform enough to travel through the constrictions and can be collected at outlet 2.

### 2.2 Device fabrication

The rapidly evolving technique of femtosecond laser direct writing and subsequent wet etching in bulk transparent dielectrics allows unprecedented 3D design freedom[19] with high spatial resolution,[20] making it a powerful tool for microfluidic and micro-optic applications. Furthermore, there is no requirement to seal the top surface of microfluidic devices when compared to photo and soft lithographic microfabricated devices. The technique involves the irradiation of bulk substrate material using focused, sub-bandgap femtosecond laser pulses leading to enhanced chemical etching selectivity.[21] In recent years, novel applications have been successfully demonstrated using femtosecond laser direct writing in the fields of integrated optics,[22] optofluidic LOC devices[17] and micromechanical systems.[23]

The device was written using 460 fs pulses at a repetition rate of 500 kHz from a commercial Yb-doped master oscillator power amplifier laser system (IMRA America FCPA μ Jewel D400) at 1047 nm, focused inside a fused silica substrate (Corning 7980, UV Grade) using a 0.4 NA (x20) aspheric objective lens. Accurate translation of the substrate through the laser focus was controlled using Aerotech Automation 3200 multi-axis air bearing stages. We applied the polarisation sensitive wet etching property of fused silica and fabricated the device in separate components in order to preserve their post etch aspect ratio. Each component was written using optimum laser writing parameters to achieve controlled etch rates. Optimising the parameters allowed us to achieve etching rate selectivity one order of magnitude higher than those reported by Hnatovsky *et al.*[14] The details of the optimisation process will be communicated separately.

Optical micrographs of various components of the device before and after the etching process are shown in Fig. 2(a)–(c).

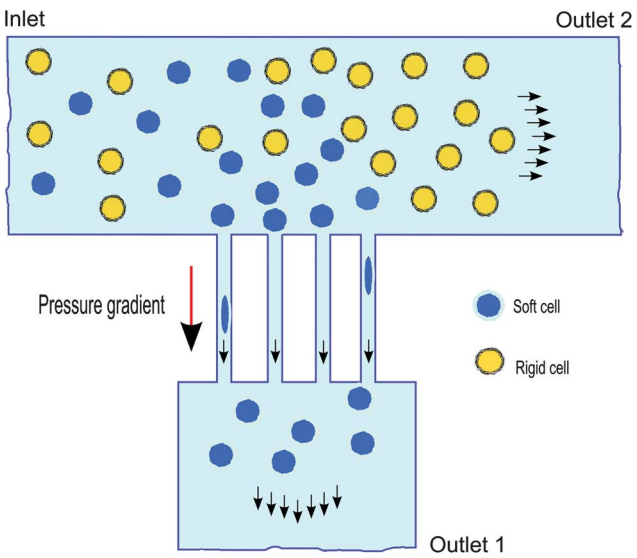


**Fig. 1** Schematic showing the working mechanism of the device. A pressure gradient applied between the two microchannels allows the relatively softer cells to squeeze through the constrictions to be collected at outlet 1.

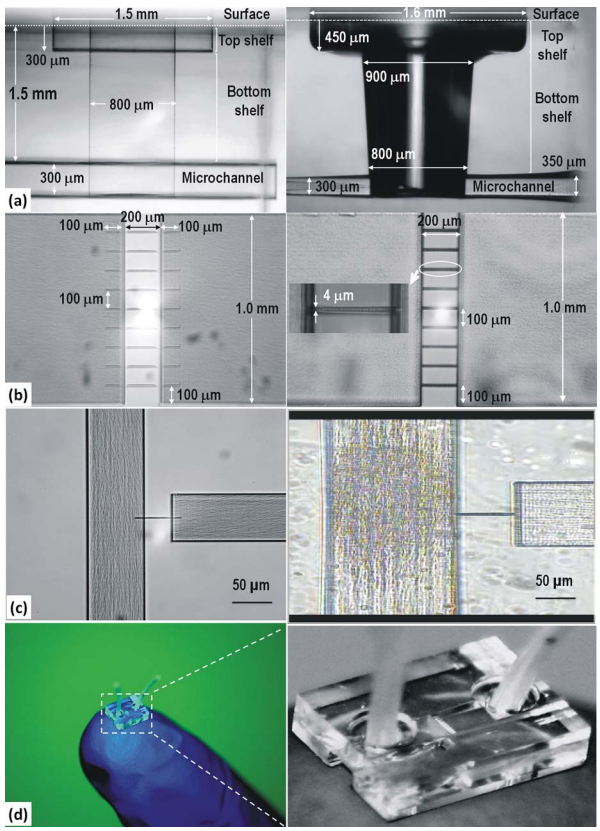


**Fig. 2** (a–c) Optical micrographs showing the components of the device before etching (left) and after etching (right) with HF at 13.3% (v/v) dilution for 4.5 h. (a) The inlet system viewed side-on. (b) Top view of the constriction array. (c) Top view of the T-junction. (d) The device on a fingertip with a magnified view shown alongside.

The inlet ports shown in Fig. 2a have been designed in a concentric cylindrical pattern with an outer diameter of 1.5 mm, inner diameter of 750 μm and a depth of 1.6 mm. They were written using circularly polarised 650 nJ pulses at a translation speed of 4 $mms^{-1}$. Fig. 2b and 2c show the microchannels with constrictions that have been fabricated in a straight and T-junction arrangement respectively. The channels with a cross-section of 1 mm × 300 μm in Fig. 2b were fabricated using 650 nJ pulses at 2 $mms^{-1}$. The microchannels forming the 'T' in Fig. 2c have been designed with a cross-section of 100 μm × 100 μm and were also written using 650 nJ pulses at a translation speed of 2 $mms^{-1}$. The electric field vector of the laser pulses was maintained perpendicular to the translation direction at all times in order to ensure appropriate etching selectivity of the laser written microchannels. The constrictions were written using a single laser scan at the junction of the two microchannels using 270 nJ pulses at a translation speed of 0.1 $mms^{-1}$. In order to minimize unwanted mechanical forces on the cell by forcing them to remain deformed for an extended period of time, the maximum length of the constrictions is set to 200 μm. As imaging is to be performed from the bottom surface of the substrate, the network of channels were fabricated at a depth of 400 μm. Chip-to-world interfacing is achieved by linking the input and output arms of the device to cylindrical inlet ports which can be directly accommodated without the need of external adapters. Platinum cured silicone tubing (VWR) with an outer diameter of 640 μm and inner diameter of 300 μm can be directly inserted into the ports as shown in Fig.2d.

The fused silica substrate with the laser written structures was subsequently etched in an ultrasonic bath using hydrofluoric acid (HF) at 5% aqueous dilution for 11 h. The long etch time at 5% dilution can be attributed to the fact that access to the laser modified structures gets increasingly difficult as the etch profile ingresses deeper into the substrate. This issue was addressed by increasing the concentration to 13.3% (aq.), which subsequently reduced the etch time to 4.5 h without compromising the aspect ratio of the laser written structures. It was observed that optimum selection of the length of the microchannels is critical to ensure that etchant arrives at the constriction from all routes at approximately the same time in order to avoid over etching the structures.

Once etched, the device was rinsed in an ultrasonic cleaner using deionised water followed by acetone and IPA for 30 min to remove any residual traces of HF inside the microchannels. A second sacrificial etched device was ground back and polished in order to reveal the cross-section of the constriction. It was found that the constriction was slightly elongated along one axis. As shown in Fig. 3b, the longer axis was measured to be 8μm and the shorter axis 4 μm.

## 3. Device performance

We investigated the throughput of the device and subsequently, the viability and size distribution of cells within the population which have travelled through the constrictions. A T-junction device with a single constriction as shown in Fig. 2c and Fig. 3a was used to examine if the femtosecond laser direct writing and selective etching method produced an optimally sized

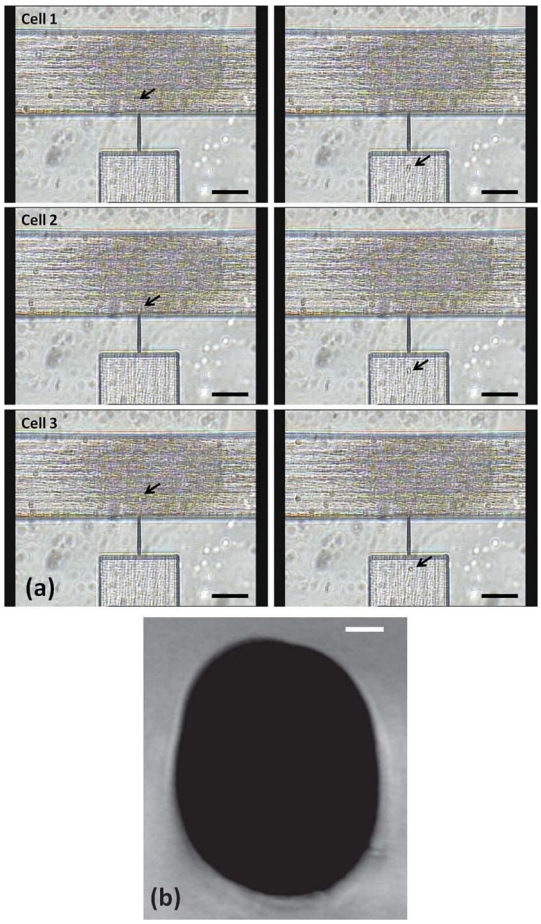


**Fig. 3** Optical micrographs of the single constriction T-junction device. (a) The HL60 cells can be clearly seen after they pass through the constriction (see supplementary material). Scale bar - 50 μm (b) Cross-sectional view of a constriction. Scale bar represents 1 μm.

constriction for cells to squeeze through and exit from in an unaltered state. Human promyelocytic leukemia (HL60) cells were chosen since they need simple maintenance *in vitro* and grow as single-cell suspension cultures without the tendency to clump or adhere to plastic or glass and are also known to possess a somewhat elastic cytoskeleton that is not uniform within a population.[24] Sample injection into the microchannels and flow rates were controlled by using a microfluidic syringe infusion pump (WPI, SP100i). Sample collection reservoirs were placed at the outlet ports of the device, which was then placed on an inverted microscope platform (Olympus IX series). The microchannels were initially flushed using phosphate-buffered saline (PBS) in order to remove any residual water in them. The device showed lag free response to external changes in flow rates ranging from 1.67 μL to 1 mL $min^{-1}$, indicating that the chip-to-world interfacing is leak free and able to withstand high fluid pressures.

The HL60 cells cultured in DMEM (Invitrogen) growth media supplemented with 20% fetal bovine serum (FBS), 2mM glutamine and 100 units of Penicillin and 100 μg of streptomycin per mL were injected into the T-junction device through the inlet port at a constant flow rate of 0.5 mL $min^{-1}$. Prior to this, a sample of the cells from the same suspension was used to

 

measure the cell size under a microscope, using 3 μm diameter microspheres as a control. The average size of healthy looking cells was obtained to be 11.7 μm ± 1.1 μm with a standard deviation of 1.09 for 25 cells. The output microchannel for outlet 1 was maintained at a lower pressure using an open ended syringe. Importantly, the constriction was found to be of optimum cross section to enable deformation of the cells during transit. Fig. 3a shows snapshot images where the cells can be seen entering the constriction and then in the output microchannel travelling towards outlet 1 after passing through the constriction.

The results indicate the possibility of separating a heterogeneous population of cells with varying degrees of elasticity into enriched populations of cells with elasticity above a certain threshold using a monolithic device fabricated by fs-laser direct writing. However, such an application would only be useful for practical purposes if the populations of cells at the output reservoirs are not damaged by the process of passage through narrow constrictions. In order to analyse if this is the case and also to obtain a high throughput, the design was consequently multiplexed into a straight channel device with an array of constrictions as shown in Fig. 2b. The microchannel dimensions were increased to 1000 μm × 300 μm × 3100 μm. A two dimensional array of 18 constrictions, each of length 200 μm and width 4 μm was fabricated in the device. The cell viability assessment was performed on the output population of the device using a commercial fluorescence activated cell cytometer (BD FACSCalibur™).

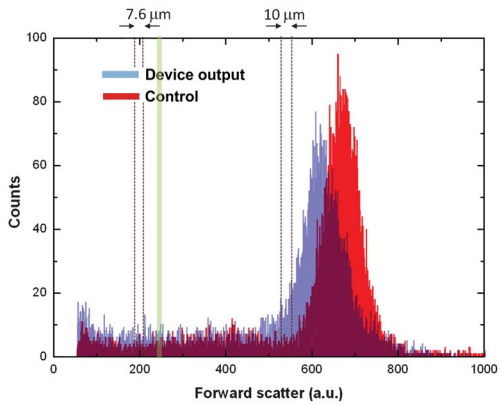


**Fig. 4** Forward scatter histogram plots obtained from the fluorescence activated cell sorter (FACS) live/dead analysis, showing the position of live cells. Data from the sample that passed through the device is plotted in blue. The control data is plotted in red. The overlaid plots reveal that the healthy population in the control lies between forward scatter values of ~550 and ~800 and makes up 78.6% of the total number of events detected. In the device output, this population lies between forward scatter values of ~480 and ~780 and constitutes 64.3% of the total events. A relative drop in maximum counts is observed in the device output. A shift towards lower forward scatter is also observed in the distribution of the device output indicating a reduction in average size of the viable cells. A corresponding increase in the device output is observed in sub-200 values representing debris from fragmented cells. The vertical dashed bands represent the size of 7.6 μm and 10 μm microspheres that have been used for size calibration. The green vertical band represents the microchannel size of 8 μm.

Prior to introducing cells into the device, they were stained with the BD™ cell viability kit consisting of Thiazole Orange (TO) and Propidium Iodide (PI). A constant flow rate of 167 μL $min^{-1}$ was used to deliver the stained HL60 cell sample through the device. A comparative FACS analysis was then carried out using a control sample of stained HL60 cells which were not sent through the device. Fig. 4 shows a comparison of the forward scatter results, representing cell volume, obtained in both control and sample cases and Fig. 5 shows the respective dot plots showing forward scatter *versus* side scatter (granularity). The fluorescence plots showing TO and PI content for this data is included as supplementary information.

A size calibration was performed in order to compare the relation of the viable cell size distribution with the constriction size. Microspheres of known size (7.6 μm and 10 μm) were introduced into the FACS and their forward scatter position noted, as shown in Fig. 4 and Fig. 5a–5b. The relative position of the constriction size is also indicated. The number of total gated events (30 000) in the device output was kept equal to that of the control.

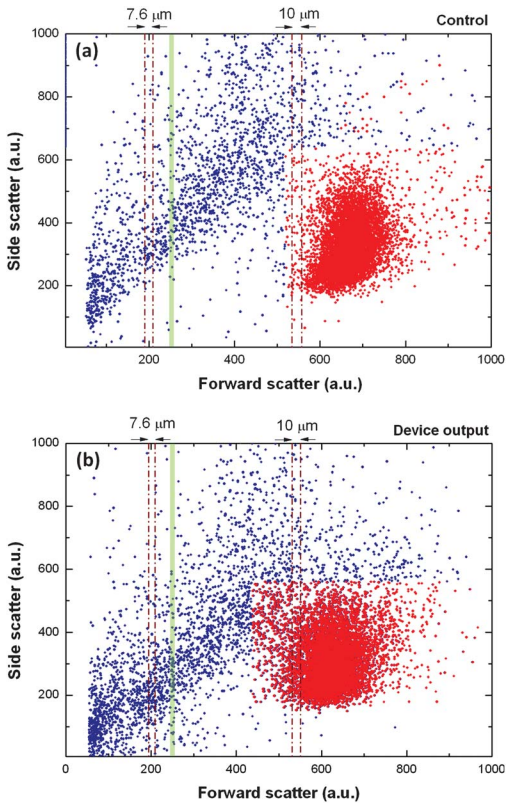


**Fig. 5** Dot plots showing variation of side scatter (SSC) against forward scatter (FSC) after the FACS live/dead analysis. Red dots represent cells stained with Thiazole Orange (TO) (representing all cellular material) while blue dots represent cells that took up Propidium Iodide (PI) (representing dead and injured cells). (a) Dot plot of side scatter against forward scatter of the control. (b) Dot plot of side scatter against forward scatter of the device output. The fluorescence FACS plots for this data is included as supplementary information. The vertical dashed bands represent the size of 7.6 μm and 10 μm microspheres that were run through the FACS for size calibration. The green band represents the microchannel size of 8 μm.

The healthy cells in the FACS histogram (Fig. 4) and dot plots (Fig. 5) correspond to the events in the fluorescence plots (see supplementary information) that show high TO content but low PI content (R1) (viable cells). In Fig. 5a, these cells are represented by a dense population of cells with x parameter values between ~550 and ~800 as marked by the red gated region in Fig. 5. These cells, comprising of 78.6% of the total gated events in the control (Fig. 5a) are almost certainly healthy due to high TO content, low PI content, large volume and low levels of granularity and therefore this population forms our region of interest. In terms of size, this population also agrees with the measured cell size of 11.7 μm ± 1.1 μm. In comparison, the data obtained from the stained HL60 cells after being sent through the device revealed 64.3% of the total gated events to be within the region of interest. In addition, compared to the control, a slight increase in counts is observed in the device output data at low levels of forward scatter (<200). These events also showed low levels of both TO and PI in the fluorescence plots (see supplementary information). This indicates an increase in the number of objects much smaller than the average size of healthy cells and is attributed to large cells being damaged during their travel through a constriction, in addition to some small viable cells. Thus, in Fig. 4 and Fig. 5a–5b all forward scatter objects with a value <200 can be considered as debris. This region is gated (R3) in the fluorescence plot and showed an increase from 1.9% in the control to 7.8% in the device output.

As shown in Fig. 4, this is complemented by a lowering of the maximum counts in the device output when compared to the control indicating a reduction in the number of healthy cells. A shift towards lower forward scatter is also observed in the distribution of the device output, indicating that the average size of viable cells is smaller when compared to the control. Furthermore, a number of cells in the control with larger size as shown in Fig. 5 were found to be absent in the population of cells which had travelled through the device. This observation indicates a potential size selectivity application of the constriction array. The minimum PI threshold in region R2 was selected at a slightly higher value than the maximum PI fluorescence in R1. The region R2 consists of dead and injured cells and makes up 19.5% in the control which rises to 27.9% in the device output. Events in R2 showing high TO as well as high PI content are attributed to large cells whose membrane has been compromised. It is clear from Fig. 5a and 5b that a large fraction of cells had to deform to go through the constrictions.

The passage of a single cell through a constriction is depicted in Fig. 6. The cell has a diameter of ~12 μm and can be seen to deform as it travels through a constriction with 4 μm × 8 μm cross-section and a length of 200 μm. We estimate that around 150 cells per minute travelled through a single constriction, as a total of about 30 000 cells passed through the 18 constriction array in 11 min, with 81% of the collected cells viable. The results indicate that a small population of cells does suffer damage and disruption of cellular integrity after passing through the constrictions, as expected. However, majority of the healthy population remain viable after travelling through the device and can potentially be grown in culture. This result is promising for cellular diagnostic, therapeutic and point of care applications.

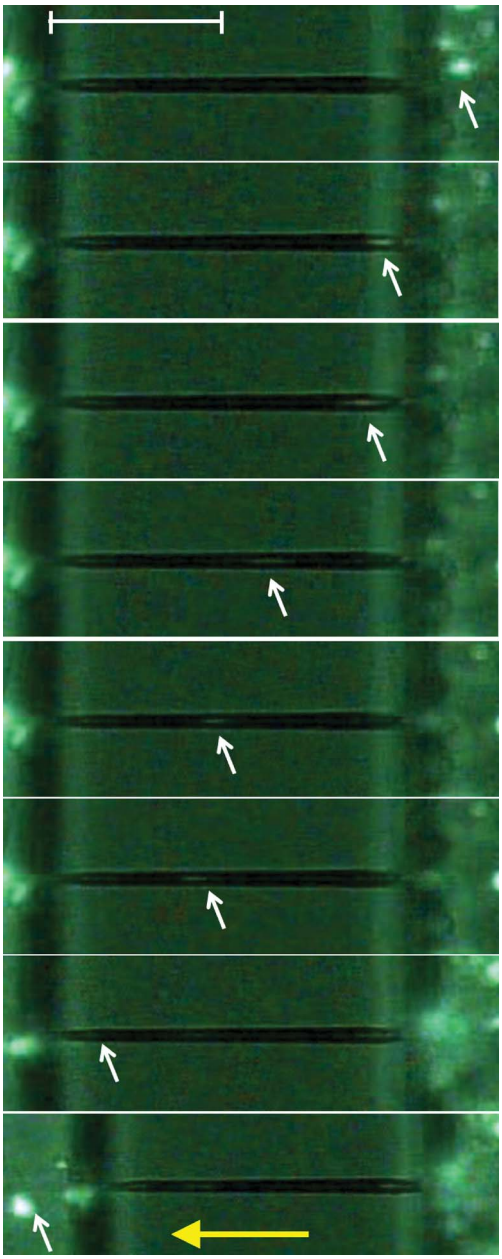

**Fig. 6** Fluorescence images showing the deformation of a single cell as it travels through the constriction in the multi-constriction device. The scale bar represents 100 μm. The white arrows show the position of the cells. The yellow arrow indicates flow direction.

## 4. Conclusions

The work presented here introduces a proof-of-principle femtosecond laser written device capable of sorting cells and collecting viable cell populations. In addition, the possibility of creating etched structures embedded in fused silica with large differences in aspect ratio is demonstrated for the first time.

The technique of femtosecond laser direct writing also presents the prospect of creating low loss optical waveguides in dielectric substrates. We are also investigating ways to optimise the device into a high-throughput, cell separator platform which includes looking into the design of novel geometries. The future version of

 

this reported device is envisioned to be a high throughput optofluidic biochip offering cytometric capability with potential applications in cancer research, regenerative medicine, affinity biosensing, cell migration, immunology and studying stress response behaviour at cellular level.

## Acknowledgements

The authors wish to acknowledge the Bioprocessing Research Industry Club (BBSRC) for facilitating this research and EPSRC (grant number EP/G030227/1) for the IMRA FCPA μJewel femtosecond laser MOPA system. The authors also wish to acknowledge Kevin Prior for facilitating the HF etching capabilities of the group and Peter Heron for prompt technical support. DC gratefully acknowledges funding from the Heriot-Watt Life Sciences Interface theme. WTR acknowledges funding from EPSRC.

## Notes and references

1 G. M. Whitesides, *Nature*, 2006, **442**, 368–373.
2 M. A. Unger, H.-P. Chou, T. Thorsen, A. Scherer and S. R. Quake, *Science*, 2000, **288**, 113–116.
3 J. P. Urbanski, W. Thies, C. Rhodes, S. Amarasinghe and T. Thorsen, *Lab Chip*, 2006, **6**, 96–104.
4 P. S. Dittrich and A. Manz, *Nat. Rev. Drug Discovery*, 2006, **5**, 210–218.
5 A. Tourovskaia, X. Figueroa-Masot and A. Folch, *Lab Chip*, 2005, **5**, 14–19.
6 S. K. Sia and G. M. Whitesides, *Electrophoresis*, 2003, **24**, 3563–3576.
7 F. Lautenschlager, S. Paschke, S. Schinkinger, A. Bruel, M. Beil and J. Guck, *Proc. Natl. Acad. Sci. U. S. A.*, 2009, **106**, 15696–15701.
8 A. Wolff, I. R. Perch-Nielsen, U. D. Larsen, P. Friis, G. Goranovic, C. R. Poulsen, J. P. Kutter and P. Telleman, *Lab Chip*, 2003, **3**, 22–27.
9 A. Y. Fu, H.-P. Chou, C. Spence, F. H. Arnold and S. R. Quake, *Anal. Chem.*, 2002, **74**, 2451–2457.
10 A. Y. Fu, C. Spence, A. Scherer, F. H. Arnold and S. R. Quake, *Nat. Biotechnol.*, 1999, **17**, 1109–1111.
11 M. Berger, J. Castelino, R. Huang, M. Shah and R. H. Austin, *Electrophoresis*, 2001, **22**, 3883–3892.
12 M. P. MacDonald, G. C. Spalding and K. Dholakia, *Nature*, 2003, **426**, 421–424.
13 M. Yamada, M. Nakashima and M. Seki, *Anal. Chem.*, 2004, **76**, 5465–5471.
14 M. Yamada and M. Seki, *Anal. Chem.*, 2006, **78**, 1357–1362.
15 C. Hnatovsky, R. S. Taylor, E. Simova, V. R. Bhardwaj, D. M. Rayner and P. B. Corkum, *Opt. Lett.*, 2005, **30**, 1867–1869.
16 M. Kim, D. J. Hwang, H. Jeon, K. Hiromatsu and C. P. Grigoropoulos, *Lab Chip*, 2009, **9**, 311–318.
17 N. Bellini, K. C. Vishnubhatla, F. Bragheri, L. Ferrara, P. Minzioni, R. Ramponi, I. Cristiani and R. Osellame, *Opt. Express*, 2010, **18**, 4679–4688.
18 H. Schillers, M. Wälte, K. Urbanova and H. Oberleithner, *Biophys. J.*, 2010, **99**, 3639–3646.
19 R. R. Gattass and E. Mazur, *Nat. Photonics*, 2008, **2**, 219–225.
20 R. M. Vazquez, R. Osellame, D. Nolli, C. Dongre, H. van den Vlekkert, R. Ramponi, M. Pollnau and G. Cerullo, *Lab Chip*, 2009, **9**, 91–96.
21 A. Marcinkevicius, S. Juodkazis, M. Watanabe, M. Miwa, S. Matsuo, H. Misawa and J. Nishii, *Opt. Lett.*, 2001, **26**, 277–279.
22 R. Osellame, V. Maselli, R. M. Vazquez, R. Ramponi and G. Cerullo, *Appl. Phys. Lett.*, 2007, **90**, 231118.
23 Y. Bellouard, A. Said and P. Bado, *Opt. Express*, 2005, **13**, 6635–6644.
24 T. G. Kuznetsova, M. N. Starodubtseva, N. I. Yegorenkov, S. A. Chizhik and R. I. Zhdanov, *Micron*, 2007, **38**, 824–833.